

## OBSERVATIONS OF ROTATING SUNSPOTS FROM TRACE

D. S. BROWN<sup>1</sup>, R. W. NIGHTINGALE<sup>2</sup>, D. ALEXANDER<sup>2</sup>, C. J. SCHRIJVER<sup>2</sup>,  
T. R. METCALF<sup>2</sup>, R. A. SHINE<sup>2</sup>, A. M. TITLE<sup>2</sup> and C. J. WOLFSON<sup>2</sup>

<sup>1</sup>*Mathematical Institute, University of St Andrews, St Andrews, KY16 9SS, U.K.*

*(e-mail: daniel@mcs.st-andrews.ac.uk)*

<sup>2</sup>*Lockheed Martin Advanced Technology Center, Department L9-41, Building 252,  
3251 Hanover Street, Palo Alto, CA94304, U.S.A.*

(Received 19 November 2002; accepted 22 May 2003)

**Abstract.** Recent observations from TRACE in the photospheric white-light channel have shown sunspots that rotate up to  $200^\circ$  about their umbral centre over a period of 3–5 days. The corresponding loops in the coronal fan are often seen to twist and can erupt as flares. In an ongoing study, seven cases of rotating sunspots have been identified, two of which can be associated with sigmoid structures appearing in *Yohkoh/SXT* and six with events seen by GOES. This paper analyzes the rotation rates of the sunspots using TRACE white-light data. Observations from AR 9114 are presented in detail in the main text and a summary of the results for the remaining six sunspots is presented in Appendixes A–F. Discussion of the key results, particularly common features, are presented, as well as possible mechanisms for sunspot rotation.

### 1. Introduction

The Sun's photosphere is highly dynamic, with sunspots and pores often seen to form, move and disappear. They also deform and interact with other sunspots/pores. Sunspot locations are where the magnetic field passes through the photosphere and are the source of the magnetic flux of active regions. In photospheric magnetograms the flux is highly fragmented and separate magnetic fragments can be seen to move and interact with each other (Berger *et al.*, 1998).

Rotational motions of and around sunspots have been observed by many authors over many decades (Evershed, 1910; St. John, 1913; Abetti, 1932; Maltby, 1964; Gopasyuk, 1965; Bhatnagar, 1967; McIntosh, 1981). Stenflo (1969) and Barnes and Sturrock (1972), independently, have suggested that the rotational motion of a sunspot may be involved with energy build-up and later release by a flare.

With the high spatial and temporal resolution of recent satellite-borne telescopes the observations of rotating sunspots and other magnetic structures have become more frequent and easier to identify. Using the TRACE and SOHO spacecraft the rotation of magnetic fragments for an X-ray bright point has been observed by Brown *et al.* (2001), where a total single magnetic field foot-point rotation of  $130^\circ$  was seen. Observational campaigns with TRACE and SOHO/MDI have found sunspots that rotate about their centres (Nightingale *et al.*, 2000, 2001a, 2002) and the



example of AR 9114, observed from 8–10 August 2000 (and also discussed here), has been described by Brown *et al.* (2002). Initial investigations of the energisation of the twisted coronal fans (Nightingale *et al.*, 2001b), the study of helicity driven sigmoid evolution (Alexander *et al.*, 2002), and the sub-surface flows of the rotating sunspot (Zhao, Kosovichev, and Duvall, 2001) are being performed.

The rotation of the magnetic footpoints in the photosphere may be associated with the injection of twist into the corona as seen in the TRACE EUV images and as S- or inverse S-shaped (sigmoid) structures observed in soft X-rays by *Yohkoh/SXT* (Canfield and Pevtsov, 1999). These twisted sigmoids are thought to be more likely to erupt and cause flares and coronal mass ejections (CMEs). The active regions studied here exhibit a diverse array of activity, including sigmoids, CMEs, and solar flares ranging from C-class to X-class. There is still much work to be done to understand the direct relationship between the emergence, or creation, of twisted structures and the disruption of the corona as a flare or CME (see Gibson *et al.*, 2002a, b).

There is a wealth of analytical (Raadu, 1972; Hood and Priest, 1979) and numerical (Galsgaard and Nordland, 1997; Arber, Longbottom, and Van der Linden, 1999; Baty, 2000a, b; Gerrard *et al.*, 2001) work that has been performed on twisted flux tubes, and they have often been associated with observed coronal features, such as sigmoids and eruptions. Much of this work discusses the degree to which a loop must be twisted before it becomes unstable, a typical quoted value being about  $2.5\pi$  or  $450^\circ$ . However, Gerrard *et al.* (2002) have investigated the twisting of a complex magnetic topology, based on AR 9114, that requires significantly less rotation before current builds up and reconnection can occur.

This paper will discuss the observation and analysis of the rotation of seven sunspots, which were obtained by the TRACE instrument, primarily in white light. The general method of analysis will be described using the sunspot from AR 9114 as an example. The results obtained using the same analysis on the other sunspots can be found in the appendixes at the end of the paper.

Principally the method involves finding the centre of the sunspot over time, and unwrapping it to create  $r - \theta$  plots of the white-light data. From this, time-slices of the white-light observations can be found on rings of constant radii (and varying angle). The rotation of sunspot then appears as diagonal light and dark streaks of identifiable features (such as penumbral fibrils).

The gradients of these streaks give the rotation speed at different locations in the sunspot at different times. Appropriate averaging of the rotation speeds can then provide the general rotation profiles with respect to time, radius and angle.

The results of this analysis for all the sunspot examples are tabulated in the discussion along with other properties of the sunspots and their active regions (such as flaring).

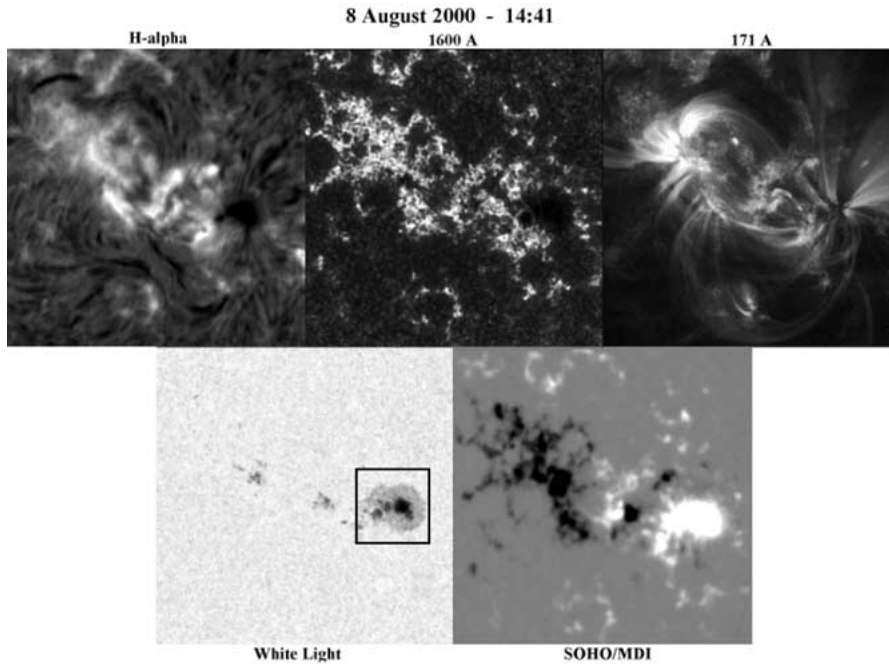


*Figure 1.* Example of sunspot data from 8–10 August 2000, showing  $H\alpha$  from Big Bear Solar Observatory, chromospheric 1600 Å band, the coronal 171 Å band, photospheric white-light band from TRACE, and a SOHO/MDI magnetogram. The box in the white-light image indicates the rotating sunspot.

## 2. The Data

The data used were taken principally from the TRACE instrument. In the active regions studied for this paper only one sunspot was analysed in each region, even though sometimes two or more sunspots might be rotating. For cases where multiple sunspots rotate, the selected sunspot's rotation was larger in magnitude than the others. In all cases, TRACE white-light data are used in the analyses of the sunspot rotation, as these give a more reliable umbral/penumbral structure than would chromospheric or corona data. The response to the rotation in the corona is shown in the 171 Å/Fe IX band (where available) in the image examples (e.g., Figure 1). Chromospheric data at 1600 Å is also shown in many cases.

For each example, a SOHO/MDI magnetogram is also shown to indicate sunspot polarity and other magnetic flux in the region. In addition,  $H\alpha$  observations from Big Bear Solar Observatory (BBSO) are included to indicate the structure in the super-penumbra.

A selection of the available white-light images is used in order to maintain a cadence which is roughly constant throughout the duration of the sunspot rotation. This cadence has typically been chosen to be between 4 and 5 min per frame.

Other observations are chosen so that they are as close as possible in time to the corresponding white-light image, normally only a couple of minutes different.

All images in a data set are derotated and cropped to follow the same region and remove lateral motion due to the rotation of the Sun. The data has been ‘despiked’ to remove cosmic ray hits as much as possible. Where necessary, the images of the same type have been renormalised to have the same effective exposure time.

### 3. Data Analysis

#### 3.1. ABOUT AR 9114

This section will detail the data analysis process using the AR 9114 data set from 8–10 August 2000 as an example.

A selection of the data for this example can be seen in Figure 1. The rotating sunspot can be seen in the white-light data along with smaller pores, some of which spiral in and merge with the sunspot. This spot is seen to rotate anticlockwise by  $150^\circ$  in the three days that it was observed. The rotating sunspot is located in the northern hemisphere about  $6^\circ$  from the equator.

As the sunspot rotated, the TRACE EUV loop structure in the corona twisted and appeared to form a sigmoid structure. This is supported by the evidence of a sigmoid in the *Yohkoh*/SXT data. At about 19:00 UT on 9 August the EUV and X-ray loops brightened indicating the potential to flare. At the time of the sigmoid brightening the GOES spacecraft registered a small C2.3 class flare that occurred between 16:00 and 20:00 UT, peaking at 16:22 UT. This flare occurred during *Yohkoh* night and so no spatial information regarding its relationship to the sigmoid is available. The *Yohkoh* data indicate the presence of post-flare loops in the region of the sigmoid but it is not clear whether the sigmoid erupted or not (Brown *et al.*, 2002).

#### 3.2. FINDING THE CENTRE OF THE SUNSPOT

Despite derotation of the data, the sunspot can still move and deform, so it is important to track the centre of the spot for each white-light image. This is done by specifying an intensity threshold, as the umbra has a low image intensity compared to the penumbra and the solar surface. Any pixel below the threshold is considered to be part of the umbra. This information is used in a centre of mass calculation to find the centre of the umbra.

#### 3.3. UNCURLING THE SUNSPOT

Once the centre of the sunspot has been found, the data are then uncurred to a polar  $r - \theta$  frame from the initial Cartesian  $x - y$  frame. The sunspot is uncurred

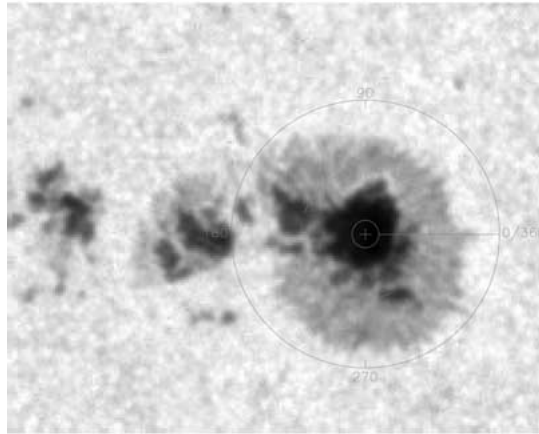


*Figure 2.* Diagram illustrating how the sunspot is uncurled. The uncurling starts at a westward pointing chord and proceeds anticlockwise about the spot. The *dashed line* indicates the location of the time-slice shown in Figure 4.

anticlockwise, starting from a westward pointing chord, as illustrated in Figure 2. The resolution used in the angular direction is  $1^\circ$ .

With this transformation any rotation will now appear as horizontal movement in the  $r-\theta$  plots. This motion can be observed by stacking a selection of  $r-\theta$  plots as in Figure 3. In this stack, the pores are seen to enter the penumbra and move to the right, indicating an anticlockwise rotation.

Alternatively, the rotation can be more effectively illustrated by extracting time-slices at fixed radii (Figure 4). This shows how the positions of features in a radial band rotate through time. The rotational motion of features can be seen as diagonal streaks. Larger features (such as the thick dark streaks made by the incoming pores) are the most obvious, but smaller features (such as penumbral fibrils) also produce these diagonal streaks. The slope of a diagonal streak (or a feature path) gives the angular speed of a rotating element.

The feature paths can be identified as having higher or lower intensity (i.e., being lighter or darker) than the background. So the features can be tracked by following local intensity maxima or minima along the specified radius. This information also provides the slope of the streaks from which the angular speed may be calculated.

It should be noted that the umbra contains fewer features that can be tracked compared to the feature-rich penumbra; this makes the umbral measurements less reliable than penumbral ones.

Moreover, bands at smaller radii contain less data. For example, a radius of  $2.5''$  (the minimum radius taken in this analysis) corresponds to a radius of 5 pixels and a circumference of approximately 32 pixels. A radius of  $5''$  will have a circumference of approximately 63 pixels and one of  $10''$  will have a circumference of 126 pixels (although in each case this is interpolated over the  $360^\circ$  box width). This means

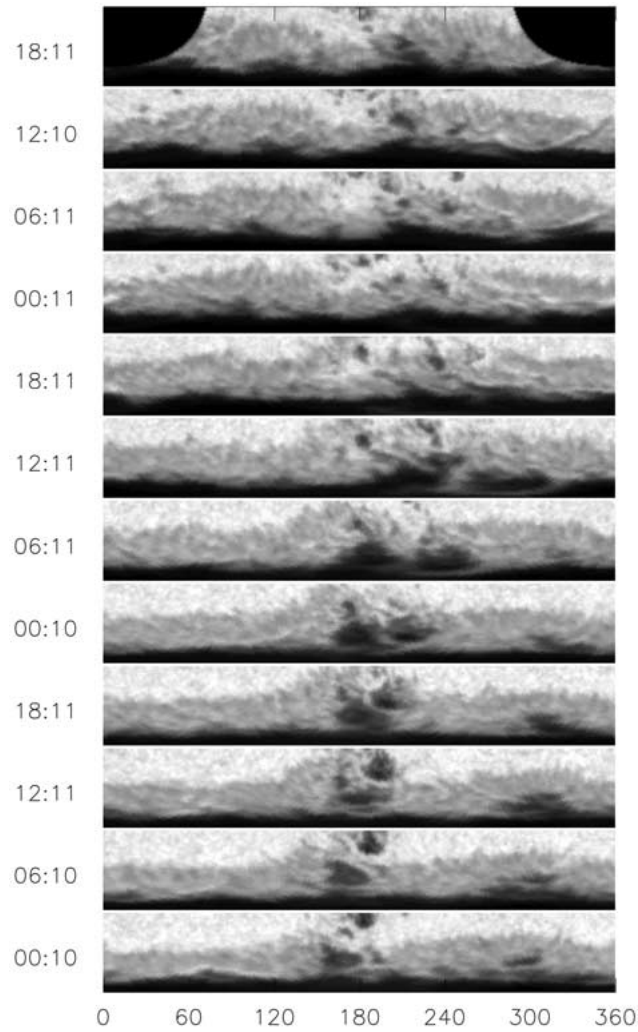


Figure 3. A selection of  $r - \theta$  white-light data plots stacked in increasing time as we progress from 8–10 August, 2000. The small sunspots can be seen to merge in to the penumbra and travel along it.

that the inner bands do not measure rotation with the same sensitivity as the outer bands, but this effect is reduced by averaging over time.

### 3.4. CALCULATING ANGULAR VELOCITIES

As there are small features throughout the data at different radii and angles, a wide spread of angular speeds is found. However, typical velocities correspond to distances smaller than one pixel (degree) between time frames. To allow for this, the speeds are averaged over  $\pm 10$  time frames (which for this example equates to  $\pm 40$  min) and  $\pm 10^\circ$ .

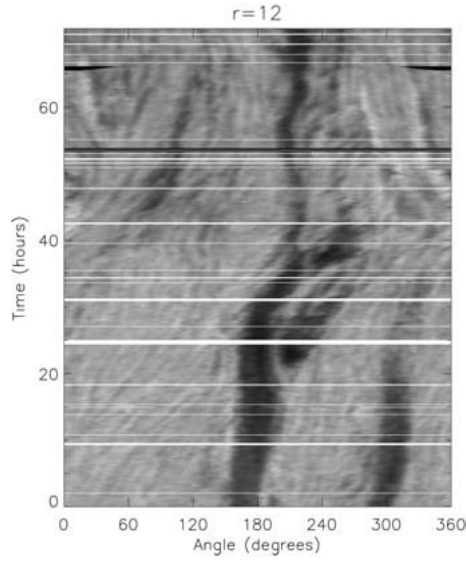


Figure 4. Time-slice taken from the white-light data at a constant radius from the centre of the sunspot. Rotation can be seen by diagonal streaks made by features as they move. The location from which this time-slice was taken can be seen in Figure 2.

So for example, the rotation speed at a radius  $r$ , angle  $\theta$  and at time  $t$  would be calculated as follows. Extract the time-slice at radius  $r$  and calculate the slopes of features in the time-slice (i.e., how far a feature moves between two time-steps). Take an average of the slopes in the region  $[\theta - 10^\circ, \theta + 10^\circ] \times [t - 40 \text{ m}, t + 40 \text{ m}]$ . This average is the rotation speed at  $(r, \theta, t)$ .

With this information the average rotation speeds with respect to time, radius and angle can be calculated.

Figure 5(a) shows the average rotation profile with respect to time. The dark line shows the average rotation of the spot as a whole including the umbra, penumbra and a little of the solar surface outside the sunspot. The lighter line shows the equivalent profile for the penumbra only. At the beginning of the TRACE observations the spot is rotating at  $0.8^\circ \text{ h}^{-1}$ , rising to just under  $2^\circ \text{ h}^{-1}$  after 35 hours before slowing down to a negligible rotation over the next day or so. Note that the beginning of the rotation was missed.

Figure 5(b) shows the average rotation profile with respect to radius. The speed is low in the umbra (between  $0-7''$ ) and rises in the penumbra to  $2^\circ \text{ h}^{-1}$  at a radius of around  $10''$  before tailing away to no significant rotation. The speed is fastest on 9 August where it reaches an average peak speed of  $3^\circ \text{ h}^{-1}$ . The rotation on 10 August is much slower.

The angular speed can be converted to a speed in  $\text{km s}^{-1}$  using the following formula:

$$v_{\text{km s}^{-1}} = \frac{726\pi}{648 \times 10^3} r_a \dot{\theta}_{d/h}, \quad (1)$$

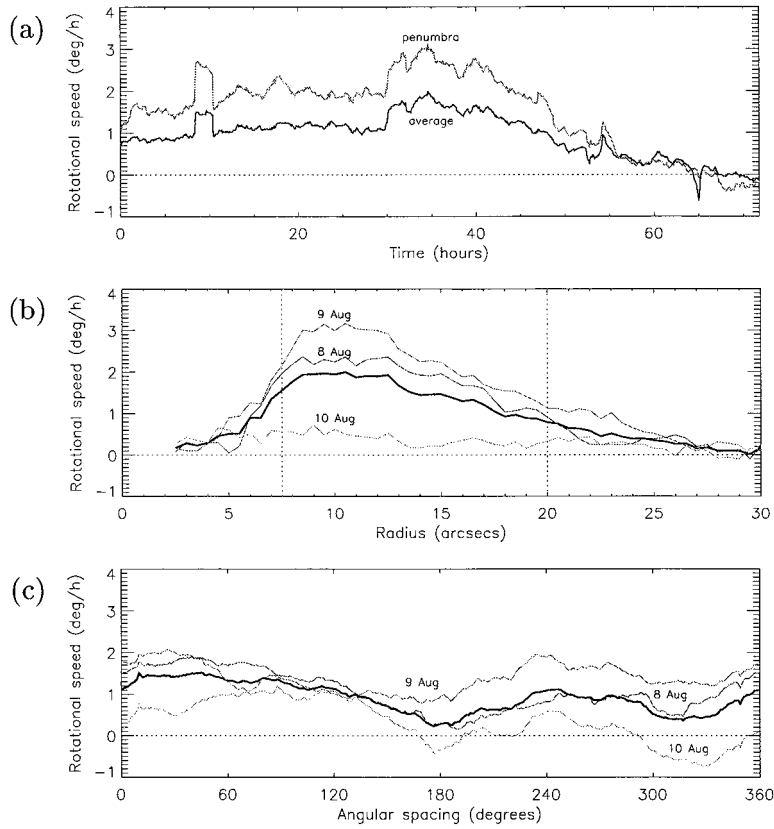


Figure 5. Plot showing the average rotation speed of the sunspot as it varies with (a) time, (b) radius, and (c) angle. Also plotted are (a) the rotation speed in the penumbra, (b) and (c) the average rotation behaviour on the individual days of the rotation. The *dotted lines* in (b) show the locations of the umbra and penumbra.

where  $v_{\text{km s}^{-1}}$  is the speed in  $\text{km s}^{-1}$ ,  $r_a$  is the radius in arcseconds and  $\dot{\theta}_{d/h}$  is the angular speed in degrees per hour. For example, an angular speed of  $3^\circ \text{ h}^{-1}$  at a radius of  $10''$  gives a plasma speed of  $0.1 \text{ km s}^{-1}$ .

The rotation profile with respect to angle (Figure 5(c)) is clearly not uniform. There is a large dip at  $180^\circ$ , which corresponds to where the two pores are starting to spiral into the sunspot. These pores are most likely disturbing the rotational flow as they maintain their shape while moving into the spot. Indeed, many of the cases in this paper show similar happenings where pores are either spiralling into or out of the sunspot.

#### 4. Results and Discussion

A mechanism for deducing the rotation of a sunspot using a geometric method with TRACE white-light data has been described, using data from 8–10 August 2000 (AR 9114) as an example. The method involves uncurling the sunspot from  $x - y$  plots to  $r - \theta$  plots, and tracking features (such as penumbral fibrils) that register as lateral movements in the  $\theta$ -direction. These motions can be best seen in time-slices of the sunspot at constant radii.

Average rotation profiles with respect to time, radius and angle can be calculated from this time-slice data. These give an impression of how the sunspot rotates in general, although specific rotation at different points in time and space will often vary greatly.

Seven cases of rotating sunspots have been studied, the example in the main text (AR 9114) and six others that are detailed in the appendixes. The key features of these cases are summarised in Table I.

The total rotation varies from between 40–200° which typically occur over 3–5 days (though this is often restricted by available data). Six cases occur in the northern hemisphere, five of which rotate anti-clockwise with one rotating clockwise. There is only one example in the southern hemisphere which rotates anti-clockwise, but the rotation is small and the rotating sunspot interacts with neighbouring spots.

This raises the question of whether there is a preference for the direction of sunspot rotation in each hemisphere? A preference has previously been found for the twist/helicity of flux tubes in the corona which has been derived from observations of sigmoids (Canfield and Pevtsov, 1999). Their preference is a left-handed twist (inverse S-sigmoids) in the northern hemisphere and right-handed twist (S-sigmoids) in the southern hemisphere. This preference would correspond to an anti-clockwise sunspot rotation in the northern hemisphere and a clockwise sunspot rotation in the southern hemisphere (Bao *et al.*, 2002).

The observations presented here are evidence of such a preference. Unfortunately, there is only one poor example in the southern hemisphere.

Of the seven cases presented, flares and/or CMEs occurred during the time of six of the observations with a diverse range of flare activity from C-class to X-class. However, probably only three of these flares/CMEs (AR 8668, AR 9077, and AR 0030) can be directly related to the rotation of the sunspots. Two of the flares (AR 9280 and AR 9354) are probably unrelated to the rotation of the sunspots and one (AR 9114) is unclear either way (see appendixes and text for the individual details). There appear to be indications that rotating sunspots contribute to the energisation of the corona, but this is still an unsolved problem.

One clear similarity between all of the rotating sunspots is the rotation profile with respect to radius. These profiles show that the sunspots have a small average rotation rate in the umbra which rises in the penumbra before tailing off to negligible rotation outside the sunspot, and so the penumbra is the part of the sunspot

TABLE I

The properties of the different rotating sunspots. The properties are date, active-region number, latitude, how much the spot rotates (in degrees), the direction of the rotation, the radius of the umbra and penumbra, the peak of the average rotation speed with respect to radius (PAR), the radius at which this occurs, the peak velocity, the number of sunspots in the active region (NSAR), the class of any flare and any other features.

Date	15–18 Aug. 1999	19–21 May 2000	13–15 July 2000	8–10 Aug. 2000
Active region	AR 8668	AR 9004	AR 9077	AR 9114
Latitude	N17	N15	N12	N06
Rotation	80–120°	90–120°	70–120°	120–150°
Direction	Anti c/w	c/w	Anti c/w	Anti c/w
Umbral rad.	10"	6"	5"	7.5"
Penum. rad.	22.5"	17"	10"	20"
PAR	1.3° h <sup>-1</sup>	3.0° h <sup>-1</sup>	1.2° h <sup>-1</sup>	2.2° h <sup>-1</sup>
Rad. of PAR	12"	9"	7"	10"
Vel. (km s <sup>-1</sup> )	0.055	0.095	0.030	0.077
NSAR	1–3	4	5–7	1–3
Flare	C5.9	–	X5.7	C2.3
Feature	Sigmoid	X-point	Slinky flare	Sigmoid
Date	21–26 Dec. 2000	21–23 Feb. 2001	13–17 July 2002	
Active region	AR 9280	AR 9354	AR 0030	
Latitude	N12	S08	N16	
Rotation	60–160°	40–60°	160–200°	
Direction	Anti c/w	Anti c/w	Anti c/w	
Umbral rad.	7.5"	5"	7.5"	
Penum. rad.	17.5"	17.5"	20"	
PAR	0.8° h <sup>-1</sup>	1.4° h <sup>-1</sup>	2.0° h <sup>-1</sup>	
Rad. of PAR	11"	6"	11"	
Vel. (km s <sup>-1</sup> )	0.031	0.030	0.077	
NSAR	4–5	3–5	4–6	
Flare	C2.1	C6.2	X3.0	
Feature	–	Flares early	Flares mid-rtn	

that rotates the fastest. It should be noted that the method for deducing rotation is less accurate in the umbra for two reasons: there are fewer features in the umbra for the algorithm to track, and there are fewer data points in the umbra.

Many of the rotation profiles suggest that rotation also occurs outside the sunspot. The plotted umbral and penumbral boundaries should, however, only be taken

as a guideline. The sunspots are not perfect circles, and some penumbral features extend beyond these boundaries.

The rotation is very slow. Typical peak velocities are given in Table I and these vary between  $0.03\text{--}0.1\text{ km s}^{-1}$ , although there may be a greater variation on different days. This means that the evolution of the magnetic field in the corona due to the rotation will generally be slow as well, which has significant implications for the type of modelling that can be performed. For example, magneto-hydrostatic modelling may be considered justifiable (see chapter on MHS in Priest, 1982).

It can be seen that the fastest rotating sunspot studied here is the one in AR 9004, which is a newly formed sunspot. In fact, the merging pores that form the sunspot are also seen to rotate as they coalesce (see Appendix B), although the rotation here can not be measured using the method described in this paper.

Furthermore, the second fastest rotating sunspot studied is the one in AR 9114. During the evolution of this region (see main text), two smaller pores spiral around then merge with the rotating sunspot. This could be an indication that this is also a young sunspot.

This raises the question of whether the rotation speed of a sunspot is related to its age? Do sunspots in the process new flux emergence have larger rotation rates than older sunspots?

Unfortunately, it is generally not possible to determine the age of a sunspot using TRACE unless it is actually seen to form (such as with AR 9004). Also, many of the active regions were observed from when they rotated onto the solar disk, and the rotating sunspots were already formed. In this case, the sunspots could have formed from anything up to about 15 days prior to observation.

The final question to be raised in this paper is what causes the observed rotation of the sunspots? Two mechanisms will be discussed here: 1. photospheric flows, and 2. flux-tube emergence.

#### 4.1. PHOTOSPHERIC FLOWS

Surface velocity patterns are primarily due to a combination of the large-scale systematic flow of differential rotation and localised proper motions resulting from magneto-convective dynamics. We can effectively exclude the effects of differential rotation as the dominant source of the observed motions for two reasons: (i) The images were ‘derotated’ prior to determining the velocities, thereby eliminating the gross effects of differential rotation, and (ii) the calculated velocity expected from differential rotation for these sunspots is one to two orders of magnitude lower than the observed velocities. (See Appendix G). Furthermore, larger sunspots would be expected to rotate faster than smaller ones, as there would be a greater difference in the sidereal motions from top to bottom, which is not seen in the observed examples.

Equation (1) shows that the rotation speed in  $\text{km s}^{-1}$  is proportional to  $r_a \dot{\theta}_{d/h}$  and for AR 9114 it peaks at about  $0.1 \text{ km s}^{-1}$ . Referring to Table I, it can be seen that all of the peak velocities observed are within an order of magnitude of this value. This is fairly small for photospheric speeds, but by no means unacceptable. Local shearing is expected to occur in the region of the outer penumbral boundary.

Differential rotation would give rise to a hemispheric preference to the direction of the rotation. However, local shearing would be unlikely to do so.

#### 4.2. FLUX-TUBE EMERGENCE

This mechanism involves the direct emergence of a twisted flux-tube, often called an  $\Omega$ -loop, (e.g., Magara and Longcope, 2001), where the photospheric ‘footprints’ are observed to rotate as the flux-tube emerges. In this case, the sunspot dynamics are governed by the twist and emergence rate of the sub-photospheric flux-tube. Additional consequences of this scenario include the presence of a corresponding anti-rotating partner foot point of the opposite polarity to the observed sunspot and the coordinated separation of the rotating foot points as the flux-tube emergence proceeds. While most of the observations described in this paper do not display such bimodal behaviour, it cannot be completely dismissed because of the limited field of view of TRACE, and the action of photospheric dynamics over days to weeks that could separate the two polarities and severely limit the ability to identify the opposite polarity structures associated with our rotating sunspot.

Numerical MHD simulations would have to be performed to investigate this possibility further. Questions that could be addressed are: whether the observed rotation profiles with respect to radius could be reproduced; how the amount of sub-surface twisting effects the rotation rate; and how much the sunspot rotates in total.

Further analysis will be required to determine the primary mechanism for the cause of the observed rotating sunspots.

It should be noted that there is an additional geometric rotation due to the line of sight projection of sunspots on the Sun (Appendix H). This geometric rotation can be as much as a few degrees per day, depending on latitude, but is too small to account for the complete rotation of the sunspots detailed in this paper. However, it will always occur (even for non-rotating sunspots), and is an anticlockwise rotation in the northern hemisphere and clockwise in the southern hemisphere.

This is not as much of a problem for this work as the method for determining sunspot rotation outlined in this paper takes into account the north-south components of the rotation as well as the east-west. The geometric rotation is a purely east-west effect (more of a geometric shear than a rotation), so if it were analysed using the method in this paper, the average rotation would be smaller than the few degrees per hour quoted above.

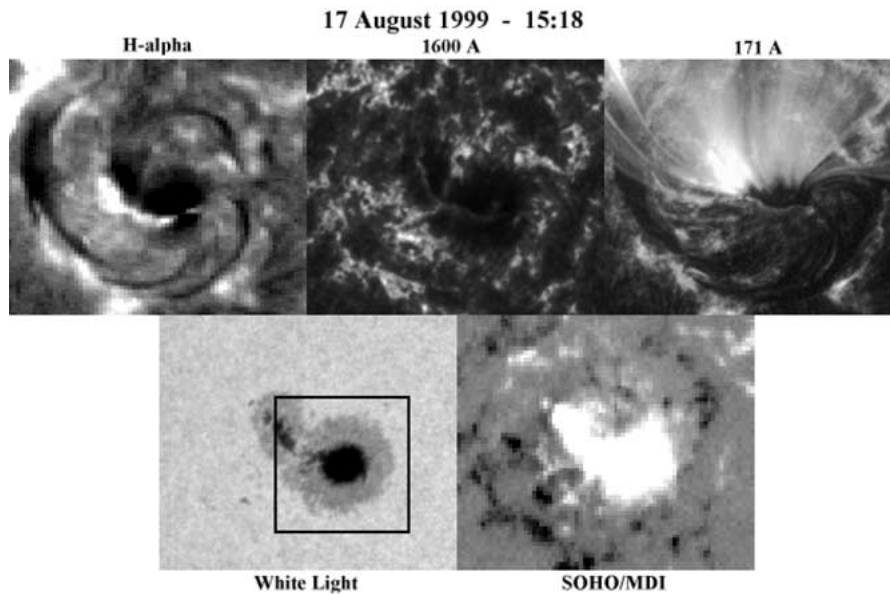


*Figure 6.* BBSO  $H\alpha$ , TRACE 1600 Å, 171 Å, and white-light observations and a SOHO/MDI magnetogram, from 17 August 1999, of an active region containing a lone sunspot that rotates. The box in the white-light image indicates the rotating sunspot.

The observations presented here provide direct evidence for the energisation of the solar corona by the emergence and/or dynamics of certain magnetic flux-tubes that appear as rotating sunspots as they pass through the photospheric surface from below and rise up into the corona. Such phenomena are important for understanding how the solar atmosphere attains the conditions necessary for the large release of energy and helicity observed in solar flares and coronal mass ejections.

#### **Appendix A. Rotating Sunspot in AR 8668 on 15–18 August 1999**

From 15–18 August 1999, a lone sunspot in AR 8668 was seen to rotate about  $100^\circ$  anti-clockwise. The spot was in the northern hemisphere,  $17^\circ$  from the equator. The sunspot was observed with the TRACE white-light, 1600 Å and 171 Å bands (Figure 6). An  $H\alpha$  image and a magnetogram are also shown.

The sunspot starts off well over toward the eastern limb, where the umbra has a keyhole shape. As it moves on to the disk centre, the keyhole separates into two separate sunspots.

Loops can be seen, in the coronal 171 Å band, to spiral into the sunspot in an anticlockwise direction (in agreement with the rotation of the sunspot), and at a larger scale a sigmoid is observed. The region flares on 17 August which GOES registers as a class C5.9 event.

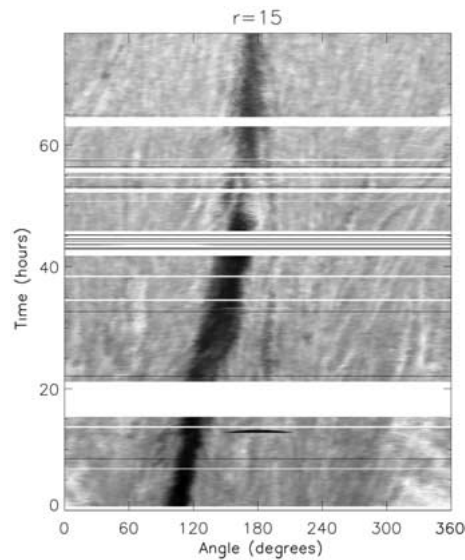


Figure 7. Time-slice of a band in the rotating sunspot's penumbra at a radius of  $15''$ . The timing begins at 00:00 UT on 15 August 1999.

A far more in depth study of this region can be found in Gibson *et al.* (2002a), although, they focus mainly on the coronal behaviour and do not discuss the rotation of the sunspot.

A time-slice of the sunspot penumbra can be seen in Figure 7. The thick dark streak is the leg of the keyhole, which can be seen to rotate about  $100^\circ$ . There are some data gaps, the largest being around 5 hours near the end of the first day.

The rotation profiles with respect to time, radius and angle can be seen in Figure 8. The profile with respect to time can be seen to be consistently slow at about  $0.5^\circ \text{ h}^{-1}$  and both the beginning and end of the rotation have been missed.

The profile due to radius shows the penumbra rotating the fastest with  $1.3^\circ \text{ h}^{-1}$  at a radius of  $12''$ . In this case there is an upturn in the rotation toward the centre of the sunspot, but, the data this close in is not as reliable as further out (see Section 3.3).

The profile due to angle is quite variable, part of which may be due to the leg of the keyhole which retains its shape against the varying profile due to radius, this will affect the rotation at the angle corresponding to the leg.

### Appendix B. Rotating Sunspot in AR 9004 on 19–21 May 2000

From 19–21 May 2000, a sunspot in a group of four in AR 9004 was seen to rotate about  $100^\circ$  clockwise. The spot was in the northern hemisphere, approximately  $15^\circ$  from the equator. The sunspot was observed with the TRACE white-light band and coronal  $171 \text{ \AA}$  band (Figure 9). An  $H\alpha$  image and a magnetogram are also shown.

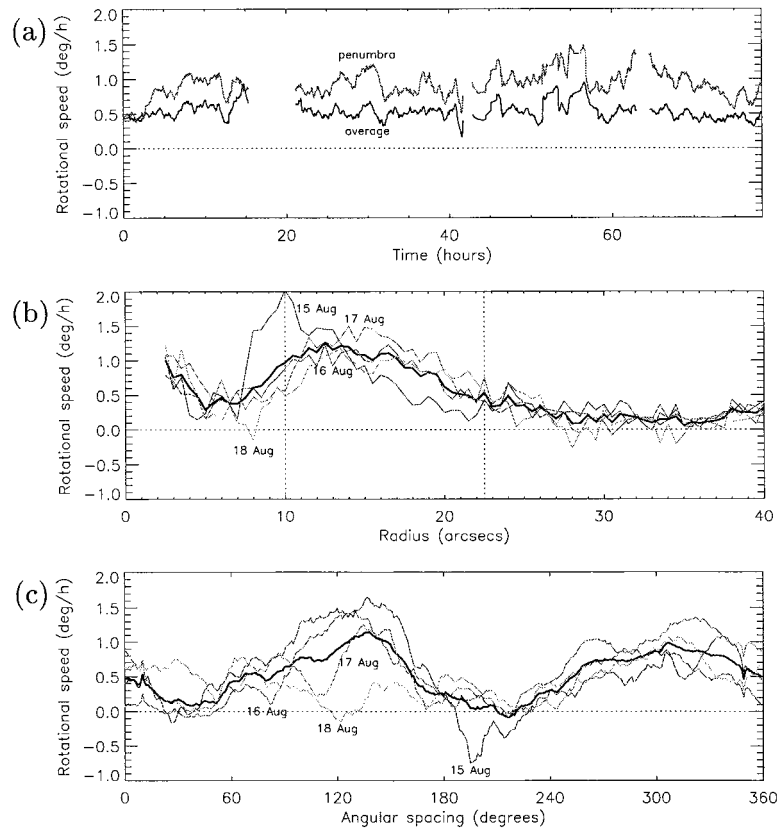


Figure 8. Plot showing the average rotation speed of the sunspot of 15–18 August 1999 as it varies with (a) time, (b) radius, and (c) angle. Additional lines show how the average rotation behaves on the individual days of the rotation.

The rotating sunspot can be seen in the  $171 \text{ \AA}$  band to have loops connecting it to the sunspots directly above and below it. The upper two sunspots are also connected by loops (Figure 9). The bottom sunspot is probably also connected to the top left sunspot, although the  $171 \text{ \AA}$  emission is weaker between these two.

These coronal loops form a crude two-dimensional  $x$ -point (at a point between the sunspot groups, see Figure 9). However, the three-dimensional magnetic structure is more complicated than this, and the  $x$ -point may well be a projection of a current ribbon.

A time-slice of this sequence is shown in Figure 10. Unfortunately, there are large gaps in this data sequence. Despite the gaps, dark features can be seen with a negative (clockwise) slope on them indicating rotations of up to  $100^\circ$ .

The slice starts at 22:00 UT on 19 May, there is a 3-hour gap before this when the spot begins to rotate. Preceding this the spot can be seen to form by the coalescing of pores, during which the spot is not well enough defined to perform the rotation analysis.

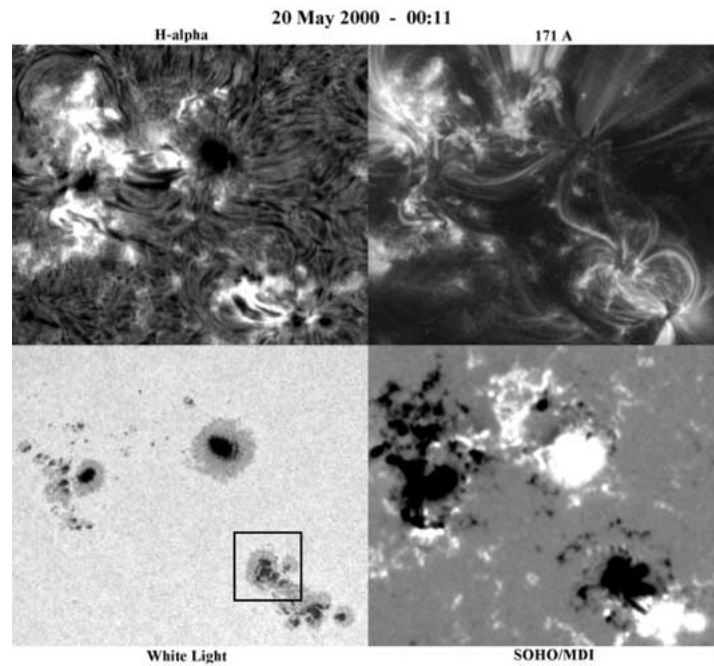


*Figure 9.* BBSO  $H\alpha$ , TRACE 171 Å and white-light observations, and a SOHO/MDI magnetogram, from 20 May 2000, of an active region containing four sunspots, one of which rotates (indicated by the box in the white-light image). The  $H\alpha$  image was taken about 6 hours before the other observations.

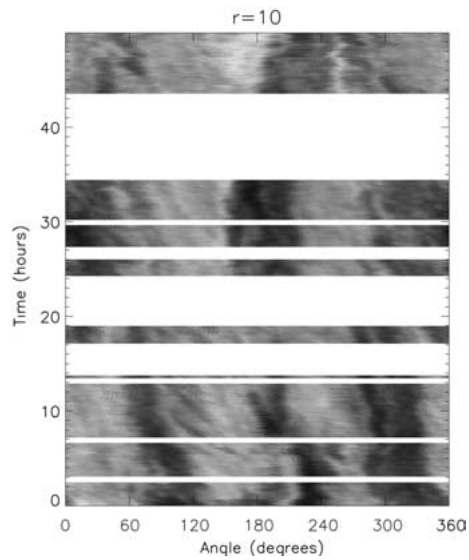


*Figure 10.* Time-slice of a band in the rotating sunspot penumbra at a radius of  $10''$ . The time starts at 22:00 UT on 19 May 2000.

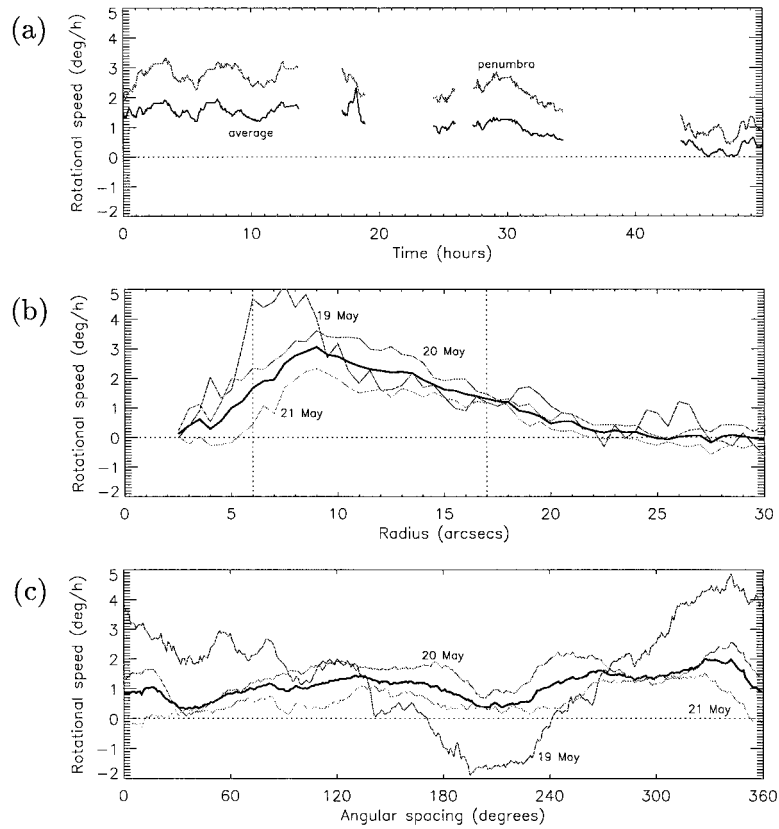
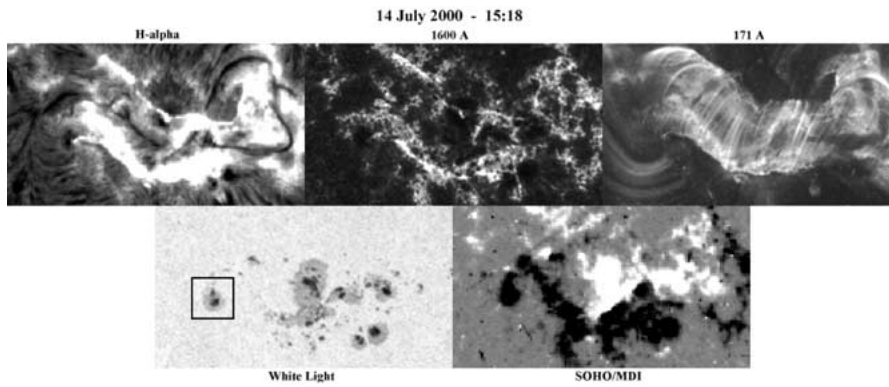


Figure 11. Plot showing the average rotation speed of the sunspot of 19–21 May 2000 as it varies with (a) time, (b) radius, and (c) angle. Additional lines show how the average rotation behaves on the individual days of the rotation.

The average rotation profiles with respect to time, radius and angle can be seen in Figure 11. The data gaps can once more be seen in the rotation profile with respect to time.

The profile with respect to radius shows that the rotation is faster in the penumbra, peaking at  $3^\circ \text{ h}^{-1}$  at a radius of  $9''$  before tailing off to nothing. The profile for the 19 May differs from this profile, but it contains only two hours (22:00 UT to 00:00 UT) of data.

The profile with respect to angle shows that, generally, all of the sunspot rotates clockwise. The exception is some deformation on 19 May which most likely corresponds to the sunspot completing its formation from a collection of pores.



*Figure 12.* BBSO  $H\alpha$ , TRACE 1600 Å 171 Å, and white-light observations, and a SOHO/MDI magnetogram, from 14 July 2000, of an active region where the leftmost sunspot rotates (indicated by the box in the white-light image). The magnetogram was taken about  $2\frac{1}{2}$  hours before the other observations.

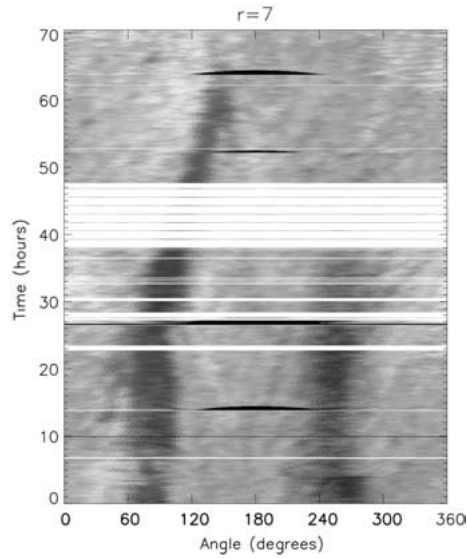


*Figure 13.* Time-slice of a band in the rotating sunspot's penumbra at a radius of  $7''$ . The timing begins at 00:00 UT on 13 July 2000.

### Appendix C. Rotating Sunspot in AR 9077 on 13–15 July 2000

From 13–15 July 2000, a sunspot in a AR 9077 was seen to rotate about  $90^\circ$  anti-clockwise. The spot was in the northern hemisphere at a distance  $12^\circ$  from the equator. The region flares on the 14th, which GOES registered as a class X5.7 flare. This flare is a well-studied event and is often referred to as the Bastille day flare or the slinky flare.

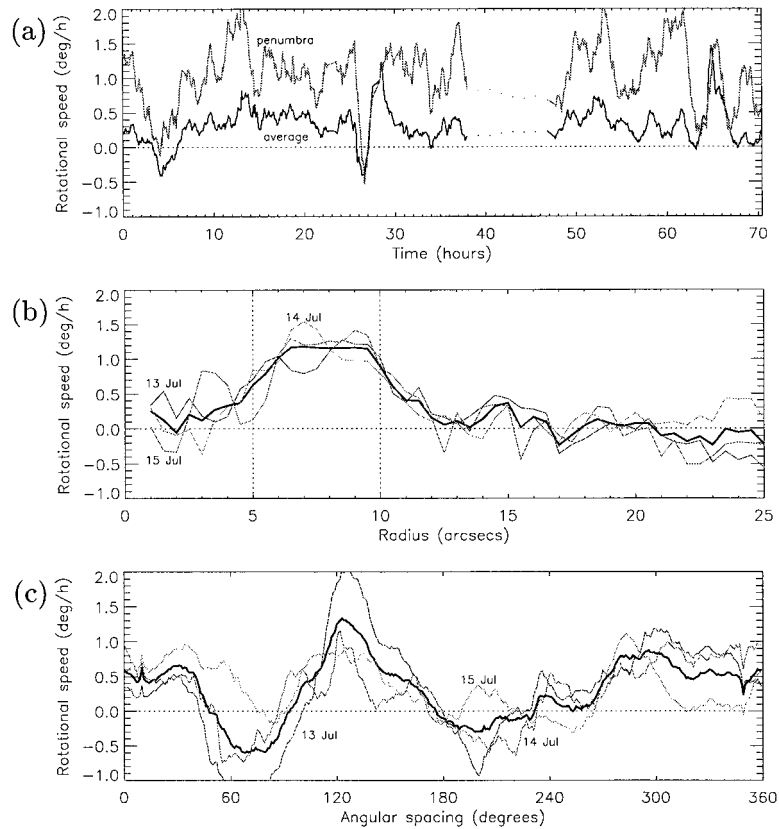


Figure 14. Plot showing the average rotation speed of the sunspot of 13–15 July 2000 as it varies with (a) time, (b) radius, and (c) angle. Additional lines show how the average rotation behaves on the individual days of the rotation.

The rotating sunspot is the trailing spot in Figure 12 located near one end of the photospheric neutral line and the nearby flare ribbons (see Liu and Zhan, 2001). It is part of a large, complex  $\beta$ – $\gamma$ – $\delta$  sunspot group that produced nearly 130 flares, including three X-class flares, the largest being the X5.7 flare of 14 July. Although the rotating sunspot probably contributed to the flare and/or CME, the latter was most likely triggered by larger, faster displacements and shearing of the more leading positive sunspots (see Somov *et al.*, 2002).

Note that the sunspot is quite small compared to previous examples and has a thin penumbral band. This gives less data for the algorithm described in this paper, which has an effect on the accuracy of the rotation profiles.

A time-slice for this sunspot is shown in Figure 13. Following the darker streaks seems to indicate that the rotation increases after 30 hours, which is about when the flare occurs. Unfortunately, there is a large data gap after this period where calculation of average rotation can't be made. This means that a portion of the rotation is not included in the average rotation profiles.

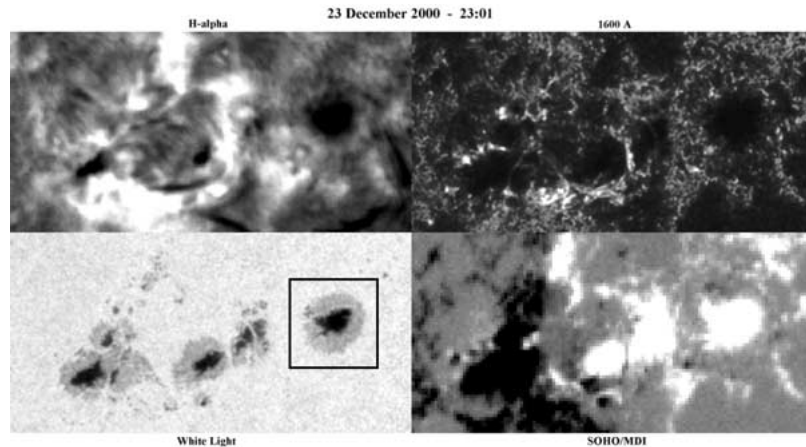


Figure 15. BBSO  $H\alpha$ , TRACE 1600 Å and white-light observations, and a SOHO/MDI magnetogram, from 23 December 2000, of an active region containing several sunspots, the rightmost of which rotates (as indicated by the box in the white-light image).

The rotation profiles (Figure 14) are quite slow, with the profile with respect to time rotating at about  $0.5^\circ \text{ h}^{-1}$  and the more erratic penumbral rotation being about  $1^\circ \text{ h}^{-1}$ . Note the data gap between 40–50 hours. The rotation speed might be faster here as the time slice indicates.

The profile with respect to radius shows the familiar characteristic where the penumbra rotates faster than the umbra. The profile with respect to angle is quite erratic, which may be due to the smallness of the sunspot (as mentioned above).

#### Appendix D. Rotating Sunspot in AR 9280 on 21–26 December 2000

From 21–26 December 2000, a sunspot in a multiple sunspot active region (AR 9280) was seen to rotate about  $120^\circ$  anti-clockwise. The spot was in the northern hemisphere,  $12^\circ$  from the equator. The active region was observed in the TRACE white light and 1600 Å bands (Figure 15). An  $H\alpha$  image and a magnetogram are also shown.

The active region starts near the limb where the rotating sunspot is actually two sunspots which coalesce. As the region moves onto the disk, the sunspot rotates, elongates and separates into two spots once more.

The region flares, and is registered as a C2.1 event by GOES. However, this may not be related to the rotation, and instead may be due to shearing in the following sunspot group.

The time-slice (Figure 16) shows that there is good data coverage for this event. The elongation of the sunspot can be seen, particularly toward the top of the time-slice, as the dark streak that strengthens after about 50 hours.

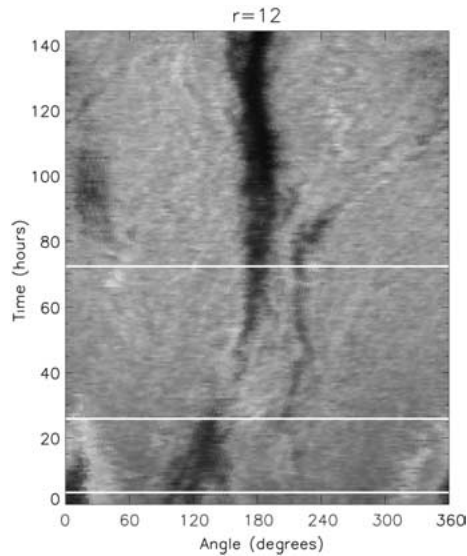


Figure 16. Time-slice of a band in the rotating sunspots penumbra at a radius of  $12''$ . The timing begins at 00:00 UT on 21 December 2000.

In this time-slice, the dark streak can be seen to rotate about  $60^\circ$ , but smaller penumbral features rotate more.

The rotation profiles (Figure 17) for this example are the slowest of the seven cases, with the average profile with respect to time staying below  $0.5^\circ \text{ h}^{-1}$ , and the corresponding rotation in the penumbra rarely going above  $1^\circ \text{ h}^{-1}$ .

The rotation due to radius shows the familiar profile of the rotation being slower in the umbra and increasing in the penumbra before tailing away to no rotation.

The rotation with respect to the angle suggests that there are two areas where minimal rotation is occurring, at  $50^\circ$  and  $200^\circ$ . This is just in front of the elongated parts (semi-major axis) of the sunspot (in the direction of rotation), and suggests that the rotation is quicker nearer the narrow part (semi-minor axis).

#### Appendix E. Rotating Sunspot in AR 9354 on 21–23 February 2001

From 21–23 February 2001, a sunspot in AR 9354 was seen to rotate about  $60^\circ$  anti-clockwise. The spot was in the southern hemisphere  $8^\circ$  from the equator. The rotating sunspot is the trailing one in Figure 18, which starts as three separate sunspots that merge and rotate.

This is a poor example as the merging and shearing of the three sunspots causes uncertainties in the rotation algorithm. To a large degree, the rotation is the product of one sunspot slipping over the other two which causes rotation to be seen predominantly at the top of the spot. This example is included because it is located in the southern hemisphere.

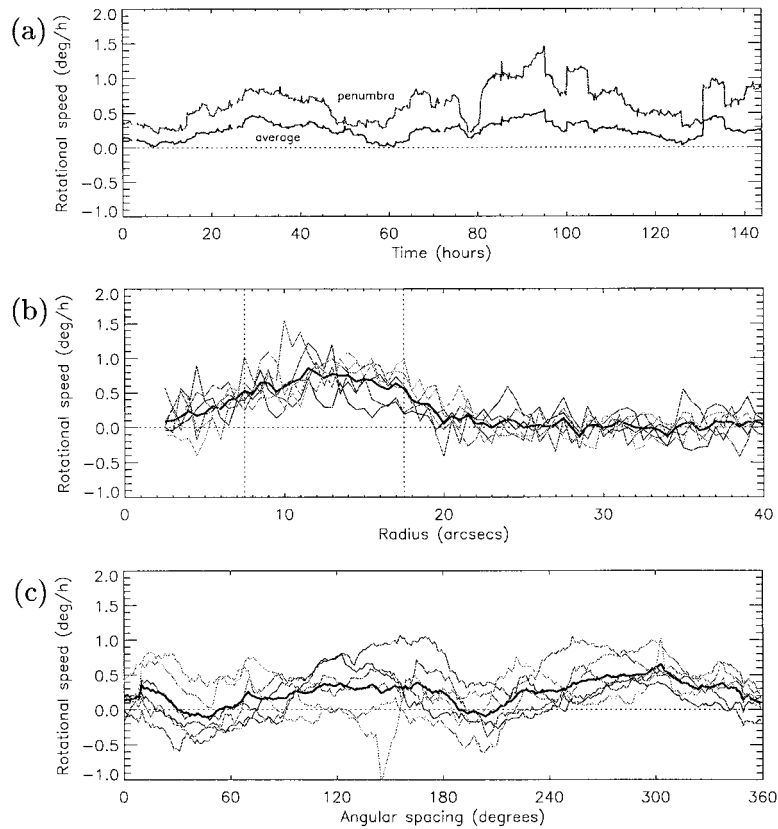


Figure 17. Plot showing the average rotation speed of the sunspot of 21–26 December 2000 as it varies with (a) time, (b) radius, and (c) angle. Additional lines show how the average rotation behaves on the individual days of the rotation.

There is a GOES class C6.2 flare observed, but, this is early in the evolution and is probably caused by the shearing and separation of the sunspot and a collection of pores rather than any rotation.

There are several data gaps, the largest being 10 hours between 50 and 60 hours into the evolution. The predominant rotation can be seen in the dark streaks in the time-slice (Figure 19) between 20 and 45 hours into the evolution.

The rotation profiles (Figure 20) confirm what has been suggested above. The profile with respect to time shows that the bulk of the rotation takes place between 20 and 45 hours, averaging about  $0.6^\circ \text{ h}^{-1}$ , while the penumbra is rotating at about  $1.3^\circ \text{ h}^{-1}$ .

The profile with respect to radius exhibits the familiar slow rotation in the umbra, rising to a peak in the penumbra then reducing to minimal rotation outside the sunspot.

The rotation profile with respect to angle shows that on average the eastern half is rotating at about  $0.5^\circ \text{ h}^{-1}$  (recall that  $0^\circ$  is a western chord and the sunspot is

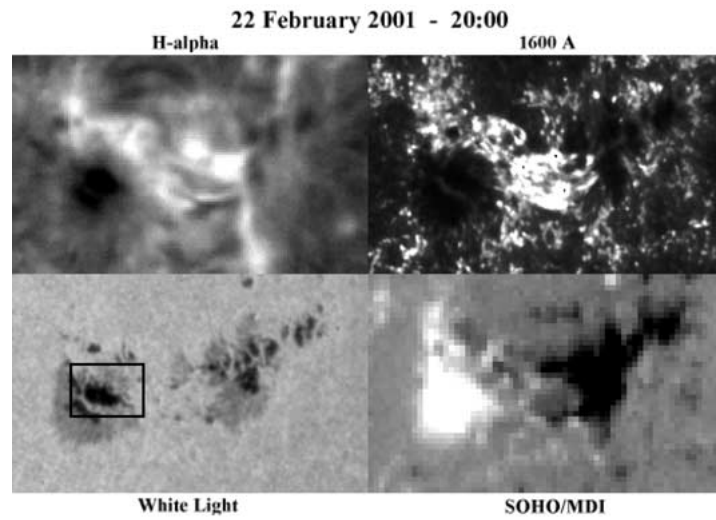


*Figure 18.* BBSO  $H\alpha$ , TRACE 1600 Å, and white-light observations, and a SOHO/MDI magnetogram, from 22 February 2001, of an active region where the leftmost sunspot rotates (as indicated by the box in the white-light image).

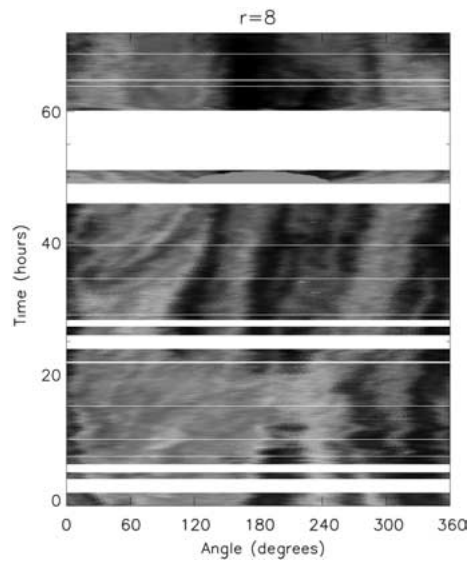


*Figure 19.* Time-slice of a band in the rotating sunspots penumbra at a radius of  $8''$ . The timing begins at 00:00 UT on 21 February 2001.

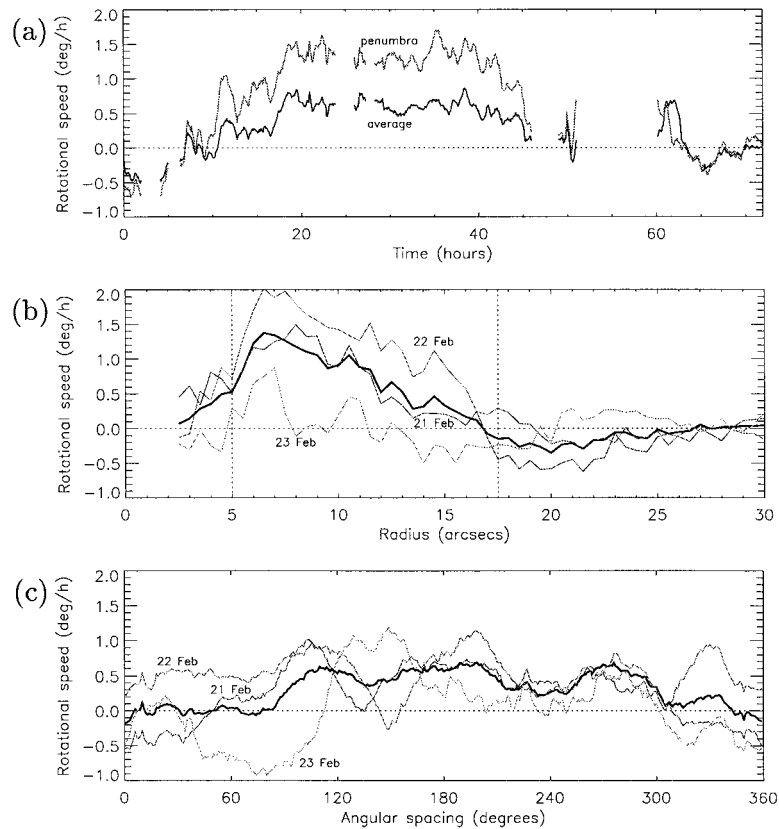


Figure 20. Plot showing the average rotation speed of the sunspot of 21–23 February 2001 as it varies with (a) time, (b) radius, and (c) angle. Additional lines show how the average rotation behaves on the individual days of the rotation.

uncurled anticlockwise). However, the negligible rotation to the west is probably due to interaction with features (e.g., pores and sunspots) in that direction.

#### Appendix F. Rotating Sunspot in AR 0030 on 13–17 July 2002

From 13–17 July 2002, a large sunspot in the centre of AR 0030 was seen to rotate about  $180^\circ$  anti-clockwise. The spot was in the northern hemisphere  $16^\circ$  from the equator.

Figure 21 shows observations from TRACE white light, chromospheric  $1600 \text{ \AA}$ , SOHO/EIT  $195 \text{ \AA}$ , SOHO/MDI and BBSO  $H\alpha$ . The sequence starts toward the limb and the region rotates onto the disk. The region flares with a GOES X3.0 event which is connected to the rotating sunspot. However, the rotation continues afterwards and the sunspot splits into two.

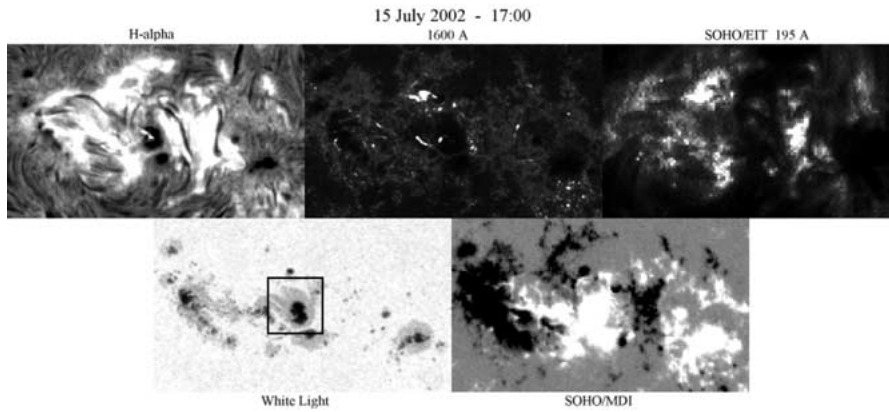


Figure 21. BBSO  $H\alpha$ , TRACE 1600 Å, EIT 195 Å, TRACE white-light observations, and a SOHO/MDI magnetogram, from 15 July 2002, of an active region where the large centre sunspot rotates (as indicated by the box in the white-light image). The magnetogram was taken about 30 min after the other observations.

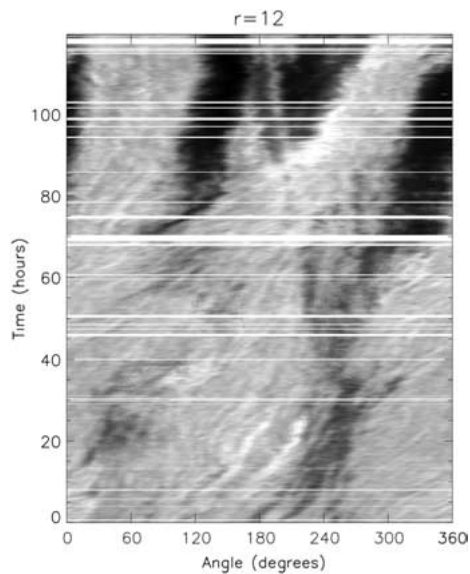


Figure 22. Time-slice of a band in the rotating sunspots penumbra at a radius of  $12''$ . The timing begins at 00:00 UT on 13 July 2002.

The time-slice (Figure 22) shows very strong rotation, and the other sunspot after separation can be seen at the top of the time-slice. Note that the data coverage for this event is very good, with no large data gaps.

The rotation profiles can be seen in Figure 23. The profile with respect to time shows that the average rotation is typically above  $1^\circ \text{ h}^{-1}$  until it slows after 80 hours, and the rotation in the penumbra is about  $2^\circ \text{ h}^{-1}$  for this time. The rotation

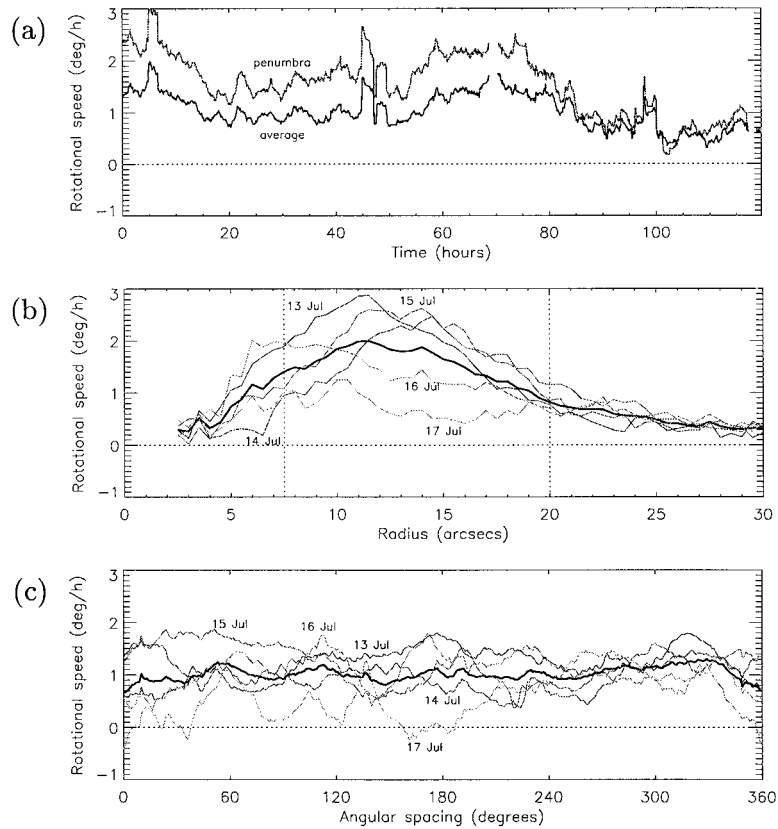


Figure 23. Plot showing the average rotation speed of the sunspot of 13–17 July 2002 as it varies with (a) time, (b) radius, and (c) angle. Additional lines show how the average rotation behaves on the individual days of the rotation.

is large at the beginning of the plot, which suggests that the start of the rotation has been missed. The sunspot would have been close to the limb at this time.

The profile with respect to radius displays the familiar curve where the umbra rotates slowly and the rotation peaks in the penumbra (at  $2^\circ \text{ h}^{-1}$ , but it reaches  $3^\circ \text{ h}^{-1}$  on 13 July).

The rotation profile with respect to angle is fairly steady at  $1^\circ \text{ h}^{-1}$ , with the daily profiles being fairly consistent with this. The only exception is for 17 July when the sunspot has split in two.

### Appendix G. Could the Rotating Sunspots be Due to Differential Rotation?

This Appendix will calculate what the speed of rotation of a sunspot would be if the rotation were caused purely by the differential rotation of the Sun being different at the northern and southern edges of a sunspot.

Differential rotation on the Sun is often described by the equation (or some modification of it) from Newton and Nunn (1951)

$$\xi = a + b \sin^2(\phi),$$

where  $\xi$  is the daily sidereal motion at latitude  $\phi$ ,  $a$  is the sidereal motion at the equator and  $b$  is a constant of the equation.

A study of the data from 1934–1944 estimates the constants to be  $a = 14.38^\circ$  per day and  $b = -2.96^\circ$  per day, although more recent studies (Ternullo, 1990) suggest that the value for  $b$  may be slightly higher. As the above equation is linear in  $b$ , the stated value above will be used as the following calculation is intended to produce an order of magnitude estimate.

The radius of the Sun is 696 Mm which gives a circumference of 4373 Mm. This means that  $1^\circ = 12.15$  Mm at the equator and gets smaller as the latitude increases. At a latitude of  $15^\circ$ , the value of  $1^\circ = 11.73$  Mm.

Consider a sunspot at  $15^\circ$  latitude with its peak rotation occurring at a  $10'' = 7.26$  Mm  $\approx 0.6^\circ$  radius. This locates the top of the sunspot at  $15.6^\circ$  and the bottom at  $14.4^\circ$  latitude. The relative axial rotation about the Sun of the bottom of the sunspot with the top is given by

$$\delta\xi = b (\sin^2(14.4) - \sin^2(15.6))$$

which, taking  $b = -2.96$ , gives

$$\delta\xi \approx 0.03^\circ \text{ d}^{-1}.$$

This can now be converted into  $\text{km s}^{-1}$  by multiplying by the value for  $1^\circ$  of rotation at  $15^\circ$  latitude, and dividing by  $24 \times 60 \times 60$  seconds in a day. This gives

$$\delta\xi \approx 4 \times 10^{-3} \text{ km s}^{-1}.$$

So the rotation speed of the sunspot with respect to its centre is half of  $\delta\xi$ , or  $v_{\text{km s}^{-1}} = 2 \times 10^{-3} \text{ km s}^{-1}$ , more than an order of magnitude less than is observed (see PAR in Table I).

This can be converted into a sunspot rotation rate by inverting the formula in Equation (1). This gives a rotation speed of  $0.057^\circ \text{ h}^{-1}$ , which is also more than an order of magnitude less than the observed rotation speeds.

### Appendix H. Geometric Effects Due to the Line-of-Sight Projection

Consider a simple model of the Sun, where effects like differential rotation are ignored and solid body rotation occurs. Place a stylised circular sunspot in the northern hemisphere, and view with the sunspot near the eastern limb, mid disk and near the western limb (Figure 24). From this, it can be seen that an anticlockwise

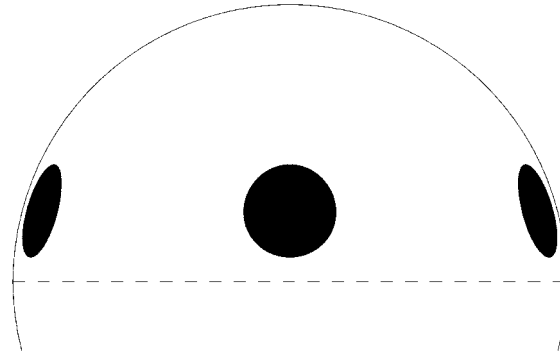


Figure 24. The projection of three identical stylised circular sunspots onto the Sun, one near the eastern limb, one at the disk centre and one on the western limb. This indicates a geometrical rotation.

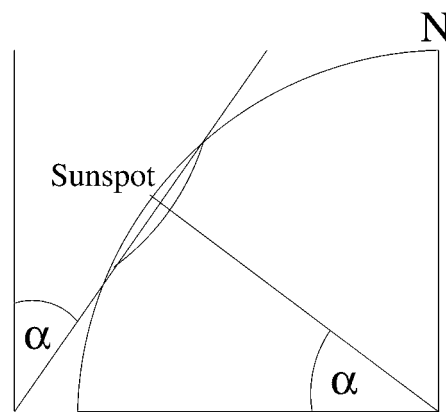


Figure 25. Diagram showing how the latitude of the sunspot relates to the angle of the sunspot with the northern axis.

geometric rotation of the sunspot has taken place due to the line of sight observing of the Sun (the rotation is clockwise in the southern hemisphere).

At the eastern limb, the angle between a top-to-bottom chord of the sunspot and the northern axis (clockwise) is the same as the angle of latitude of the centre of the sunspot (Figure 25). The same is true at the western limb, except the angle is anticlockwise to the northern axis.

So a sunspot at  $15^\circ$  latitude will have an angle of  $-15^\circ$  at the eastern limb and  $15^\circ$  at the western limb. As the Sun rotates between the two limbs, the sunspot will rotate  $30^\circ$  about its own axis. Taking the rotation period of the solid body Sun to be 30 days, the limb to limb rotation will take 15 days, giving a sunspot rotation speed of  $2^\circ \text{ d}^{-1}$ , or  $0.083^\circ \text{ h}^{-1}$ .

However, the sunspot's geometric rotation speed is actually nonlinear across the disk. The angle of inclination varies as

$$\theta = \alpha \cos \phi,$$

where  $\alpha$  is the angle of latitude and  $-\pi/2 \leq \phi \leq \pi/2$  is the variation from the eastern to western limb.

Assuming solid body rotation of the Sun in 30 days (as above),  $\phi$  can be rewritten as

$$\phi = \pi \left( \frac{t_d}{15} - \frac{1}{2} \right),$$

where  $0 \leq t_d \leq 15$  is the time in days. Combining these two equations and differentiating gives

$$\frac{d\theta}{dt_d} = \frac{\alpha\pi}{15} \cos \left[ \pi \left( \frac{t_d}{15} - \frac{1}{2} \right) \right].$$

This gives the geometric rotation of the sunspot in degrees per day.

At either limb ( $t_d = 0$  or  $t_d = 15$ ), the cosine part of this equation is small, so the geometric rotation is slow. Mid-disk, the cosine part is 1, so the geometric rotation is at its quickest, with

$$\left. \frac{d\theta}{dt_d} \right|_{\text{mid-disk}} = \frac{\alpha\pi}{15}.$$

So for the example above with a sunspot at  $\alpha = 15^\circ$  latitude, the sunspot's geometric rotation speed is  $\pi^\circ \text{ d}^{-1}$ , or  $0.13^\circ \text{ h}^{-1}$ .

This is an order of magnitude less than observed rotation speeds.

### Appendix I. Material on the CD-ROM

Animations of the data for each of the rotating sunspots discussed in this paper can be found on the accompanying CD-ROM. The sequences show the white-light observations along with the other TRACE and SOHO bands that have been discussed in each case.

### Acknowledgements

Observations in this paper were taken from TRACE, SOHO, and Big Bear Solar Observatory/New Jersey Institute of Technology. Thanks are given to the people involved with these instruments.

D. S. Brown would like to thank the Particle Physics and Astronomy Research Council for financial support. This work was supported at LMSAL by NASA under contract NAS5-38099.

### References

- Abetti, G.: 1932, *Osserv. Mem. Oss. Astrofis. Arcetri* **50**, 47.  
 Alexander, D., Nightingale, R. W., Metcalf, T. R., and Brown, D. S.: 2002, *Bulletin of American Astronomical Society, 200th Annual Meeting* **34**, Abstract 36.08.  
 Arber, T. D., Longbottom, A. W., and Van der Linden, R. A. M.: 1999, *Astrophys. J.* **517**, 990.

- Bao, S. D., Sakurai, T., and Suematsu, Y.: 2002, *Astrophys. J.* **573**, 445.
- Barnes, C. W. and Sturrock, P. A.: 1972, *Astrophys. J.* **174**, 659.
- Baty, H.: 2000a, *Astron. Astrophys.* **353**, 1074.
- Baty, H.: 2000b, *Astron. Astrophys.* **360**, 345.
- Berger, T. E., Loefdahl, M. G., Shine, R. A., and Title, A. M.: 1998, *Astrophys. J.* **495**, 973.
- Bhatnagar, A.: 1967, *Kodaikanal Observ. Bull.* **A180**.
- Brown, D. S., Parnell, C. E., Deluca, E. E., Golub, L., and McMullen, R. A.: 2001, *Solar Phys.* **201**, 305.
- Brown, D. S., Nightingale, R. W., Alexander, D., Schrijver, C. J., Metcalf, T. R., Shine, R. A., Title, A. M., and Wolfson, C. J.: 2002, *Magnetic Coupling of the Solar Atmosphere*, ESA SP-505, 261.
- Canfield, R. C. and Pevtsov, A. A.: 1999, *Magnetic Helicity in Space and Laboratory Plasmas, Geophysical Monograph* **111**, 197.
- Evershed, J.: 1910, *Monthly Notices Royal Astron. Soc.* **70**, 217.
- Fan, Y. and Gong, D.: 2000, *Solar Phys.* **192**, 141.
- Galsgaard, K. and Nordlund, A.: 1997, *J. Geophys. Res.* **102**, 219.
- Gerrard, C. L., Arber, T. D., Hood, A. W., and Van der Linden, R. A. M.: 2001, *Astron. Astrophys.* **373**, 1089.
- Gerrard, C. L., Brown, D. S., Mellor, C., Arber, T. D., and Hood, A. W.: 2002, *Solar Phys.*, **213**, 39.
- Gibson, S. E., Fletcher, L., Del Zanna, G., Mason, H. E., Mandrini, C. H., Demoulin, P., Gilbert, H., Burkepile, J., Holzer, T., Alexander, D., Liu, Y., Nitta, N., Qiu, J., Schmieder, B., and Thompson, B. J.: 2002a, *Astrophys. J.* **574**, 1021.
- Gibson, S. E., Low, B. C., Fan, Y., and Fletcher, L.: 2002b, *Bull. Am. Astron. Soc.* **34**, Abstract 36.03.
- Gopasyuk, S. I.: 1965, *Izv. Krymsk. Astrofiz. Observ.* **33**, 100.
- Hood, A. W. and Priest, E. R.: 1979, *Solar Phys.* **64**, 303.
- Liu, Y. and Zhang, H.: 2001, *Astron. Astrophys.* **372**, 1019.
- Magara, T. and Longcope, D. W.: 2001, *Astrophys. J.* **559**, L55.
- Maltby, P.: 1964, *Astrophys. Norw.* **8**, 205.
- McIntosh, P. S.: 1981, in L.E. Crom and J.H. Thomas (eds.), *Proceedings of the Sacramento Peak Observatory Conference on 'The Physics of Sunspots'*, Sunspot, New Mexico, p. 7.
- Newton, H. W. and Nunn, M. L.: 1951, *Monthly Notices Royal Astron. Soc.* **111**, 413.
- Nightingale, R. W., Shine, R. A., Brown, D. S., Wolfson, C. J., Tarbell, T. D., and Title, A. M.: 2000, *Eos Trans. AGU*, **81**, Fall Meet. Suppl., abstract SH11A-10.
- Nightingale, R. W., Alexander, D., Brown, D. S., and Metcalf, T. R.: 2001a, *Eos Trans. AGU* **82**, Spring Meet. Suppl., abstract SH11C-0724.
- Nightingale, R. W., Brown, D. S., Shine, R. A., Wolfson, C. J., Frank, Z. A., and Title, A. M.: 2001b, *Eos Trans. AGU* **82**, Spring Meet. Suppl., abstract SH41B-11.
- Nightingale, R. W., Shine, R. A., Brown, D. S., Wolfson, C. J., Schrijver, K. J., Metcalf, T. R., and Title, A. M., 2002, *Proceedings of Yokoh 10th Anniversary Meeting*.
- Priest, E. R.: 1982, *Solar Magneto-Hydrodynamics*, Kluwer Academic Publishers, Dordrecht, Holland.
- Raadu, M. A.: 1972, *Solar Phys.* **22**, 425.
- Somov, B. V., Kosugi, T., Hudson, H. S., and Sakao, T.: 2002, *Astrophys. J.* **579**, 863.
- Stenflo, J. O.: 1969, *Solar Phys.* **8**, 115.
- St. John, C. E.: 1913, *Astrophys. J.* **37**, 322.
- Ternullo, M.: 1990, *Solar Phys.* **127**, 29.
- Zhao, J., Kosovichev, A. G., and Duvall, T. L.: 2001, *American Geophysical Union, Fall Meeting 2001*, abstract SH11B-0708.